Eur. Phys. J. D **19**, 231–243 (2002)
DOI: 10.1140/epjd/e20020074

THE EUROPEAN PHYSICAL JOURNAL D
EDP Sciences

Design, simulation and application of phase plates

D. Batani[1,a], C. Bleu[2], and Th. Löwer[3]

[1] Dipartamento di Fisica "G. Occhialini" and INFM, Università degli Studi di Milano-Bicocca, piazza della Scienza 3, 20126 Milano, Italy
[2] Italtel s.p.a. Cascina di Castelletto, 20019 Settimo Milanese, Milano, Italy
[3] Max-Planck Institut für Quantenoptik, Garching, Germany

Received 23 July 2001 and Received in final form 8 January 2002

Abstract. In this paper we analyze the use of phase plates to obtain homogeneous laser intensity profiles. We studied the dependence of intensity distribution on phase plates characteristics, we obtained analytical solution for the intensity profile in the focal plane for plane waves and developed a numerical simulator to calculate the intensity distribution with a generic initial beam and at any propagation plane. We defined criteria to evaluate the quality of profiles produced by different phase plates. Finally we compared experimental results obtained at the Max-Planck Institut für Quantenoptik of Garching with our numerical simulations.

PACS. 52.35.Tc Shock waves and discontinuities – 52.38.-r Laser-plasma interactions – 52.50.Jm Plasma production and heating by laser beams (laser-foil, laser-cluster, etc.)

1 Introduction

Many applications in laser-matter interaction need an intensity distribution in the focal plane which is uniform or at least free from high intensity "hot-spots". In particular some application depends on laser energy, while the electromagnetic phase distribution does not affect the physical process. One of these is inertial-confinement thermonuclear fusion (ICF) [1,2], whose request of uniform irradiation is very high. In ICF, laser beams are used to compress and heat a little sphere of deuterium-tritium to density and temperature that can start nuclear ignition [1,2]. A high degree of spherical convergence of the fuel is required: if the energy is not uniformly deposed nuclear burning will not start, furthermore the energy efficiency of the process depends on implosion symmetry [3,4]. Symmetry is function of number and geometry of laser beams, but also of the single-beam laser-intensity distribution [5]. The focal spot intensity distribution of a single laser beam is determined by interference and diffraction effects. As previously said, these may in particular produce local hot-spots and energy concentration which then produces undesirable nonlinear plasma and hydrodynamic instabilities.

Different techniques were developed to smooth the focal spot intensity distribution and eliminate hot-spots. Kato *et al.* [6] introduced random phase plates (RPP) to scramble the phase of the beam. Ross *et al.* [7,9] extended this research by using an array of diffractive lenses: the phase zones plates (PZP). We have studied these optical devices, RPP and PZP, and analyzed the focal spot intensity distribution as a function of the parameters of phase plates. We found analytic solutions for the focal spot intensity distribution and developed a numerical simulator of electromagnetic wave propagation through these devices.

Both RPP and PZP break the spatial coherence of laser beams, reducing it, and divide the initial beam in a number of beamlets only by changing the phase of each beamlet (the intensity value is not affected). These optical devices work with a focusing lens that produces the overlapping of the beamlets in the focal spot plane. The focal spot distribution intensity is then characterized by a lot of high-intensity peaks that are smaller than the original hot-spots: if such peaks have size smaller than a characteristic length in the plasma, the target will not suffer from modulations, the intensity fluctuations being averaged by plasma thermal conduction. In particular the peak size must be smaller than the mean free path of electrons in the plasma for thermal smoothing to be effective. This can be calculated as:

$$\lambda_{\mathrm{l}} = \frac{7.2 \times 10^{12} \left(T_{\mathrm{e}}\,(\mathrm{eV})\right)^2}{n_{\mathrm{e}} \ln \Lambda}\ \mathrm{cm}, \tag{1}$$

where T_{e} is plasma temperature in eV, n_{e} is electron density, Λ is the Colombian logarithm which depends on particles collisions. Typically in the corona of laser produced plasmas $n_{\mathrm{e}} \simeq 10^{21}$ cm^{-3}, $T_{\mathrm{e}} \simeq 500$ eV and $\ln \Lambda \simeq 5$, so that $\lambda_{\mathrm{l}} \simeq 3.6 \times 10^{-4}$ cm $\simeq 4$ μm.

This allows to introduce an objective criterion for evaluating the performance and design of phase plates. In order to this, we studied the spectral distribution of

[a] e-mail: batani@mib.infn.it

intensity by Fourier transform of the focal spot intensity. The request of having an intensity distribution characterized by a lot of peaks smaller than the plasma electron mean-free-path (see Eq. (1)) can be thought as producing a high "spatial-frequency" intensity distribution (Fourier transform of focal spot intensity), where the reference spatial frequency is the inverse of the plasma electron mean-free-path. Hence, the evaluation parameter can be defined as the ratio between high-frequency and low-frequency intensity:

$$J = \frac{\int\int_{1/\lambda_l}^{\infty} \left|\tilde{I}(\alpha,\beta)\right| \mathrm{d}\alpha\mathrm{d}\beta}{\int\int_{0}^{1/\lambda_l} \left|\tilde{I}(\alpha,\beta)\right| \mathrm{d}\alpha\mathrm{d}\beta}, \tag{2}$$

where $\tilde{I}(\alpha,\beta)$ is the Fourier transform of laser intensity distribution. The better profiles are then those which maximize the value of J.

Unlike RPPs, which produce a Gaussian-like intensity distribution in the focal spot, PZPs can produce a top-hat (super-Gaussian) distribution of focal spot intensity. To analyze this PZP property and to evaluate the different performance of PZPs we then need to define another parameter, which takes into account not only the elimination of short-scale laser spikes, but also how close the average profile is to a super-Gaussian one. In order to do this, we perform a spatial filtering of the intensity profile over a distance of the order of λ_l to obtain an averaged intensity I_{filtered}, which contains the same total energy of the unfiltered intensity profile. We then consider the quadratic norm of difference between the "desired" profile (a super-Gaussian distribution) and the filtered distribution, and define the evaluation parameter as:

$$J_2 = \frac{1}{||I_{\mathrm{filtered}} - S_n||_2}, \tag{3}$$

where S_n is a super-Gaussian profile of order n:

$$S_n = \exp\left[-\left(\frac{\xi^2+\eta^2}{w^2}\right)^n\right] \tag{4}$$

(where typically we choose $n = 2$). Of course the "better" average profiles are those which maximize equation (3). In the case of PZPs then, an evaluation of PZP design can be obtained by maximizing a global evaluation parameter given by a weighted sum of J and J_2.

The two parameters J and J_2 have been used in the paper to compare different phase plates. In the final part of the paper some experimental results obtained at MPQ are shown and compared to our numerical results.

As summary, the new results contained in this paper are:

- we obtained analytical solutions for the laser intensity distribution in the focal spot with phase plates of different type and geometry;
- we have introduced an objective criterion ("figure of merit") for the evaluation of phase plate performances and design;
- we have obtained experimental results on laser intensity distribution (and laser driven shocks produced in the respective positions) and compared them with our numerical simulations.

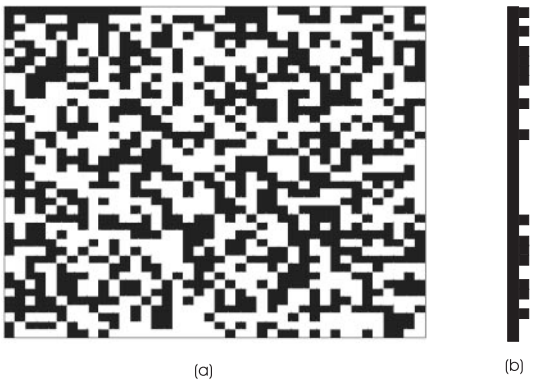

Fig. 1. Front and side view of a RPP with square zones. Black and white zones are in reality equally transparent, but white zones do not introduce additional phase, black zones introduce an additional phase of $\lambda/2$. Hence only the phase of the initial beam (and not the intensity) is damaged which explain the name of "phase plate".

2 Random phase plates

A random-phase plate consists of a two-dimensional array of transmitting areas each of which applies a phase shift randomly chosen to be either 0 or π. RPP works with a focusing lens. The RPP divides the laser beam in a number of beamlets which have a random phase shifts. The focusing lens overlaps these beamlets in the focal plane, the spot is determinate by the envelope of the beamlets. The RPP zones can be of different shapes. In the following we will discuss the case of square and hexagonal zones.

2.1 Square RPP

We calculated analytic solution for the distribution of the focal spot intensity when a plane wave travels trough a optical system composed by a focusing lens and a RPP. In this case the RPP can be considered like an array of rectangular (square in our situation, see Fig. 1) holes and we can apply the Fraunhofer approximation, the distribution of spot focal intensity is the sum of far-field solutions for the single aperture [10]. The Fourier transforms (FT) of a rectangle, is a "sinc" function. Due to FT properties, a spatial translation corresponds to a phase shift in the FT domain, and, hence, the solution is the sum of "sinc" with randomly different phases [11].

To simplify the calculations we suppose that the RPP is made of an integer number of elements, *i.e.* $D = Md$ (where D is the dimension of RPP, d is the single element dimension and M is an integer). Then the electric field

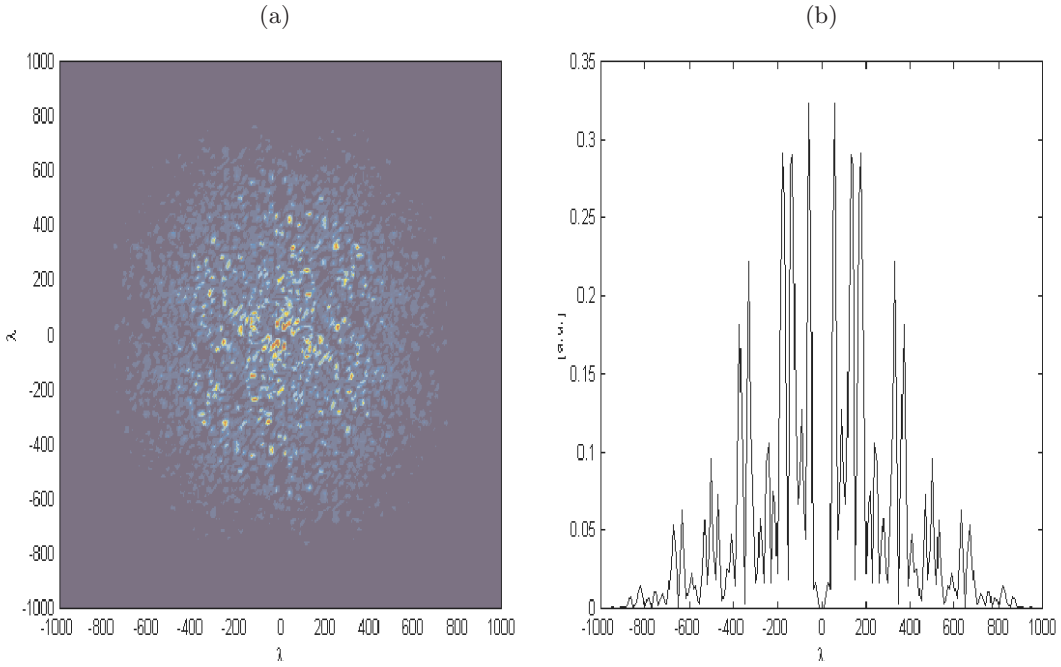

Fig. 2. Focal spot intensity distribution, analytically calculated, with a square RPP of N^2 2500 zones. RPP dimensions are $10^5\lambda \times 10^5\lambda$ and $l = 2 \times 10^3\lambda$, $f = 2 \times 10^6\lambda$. Bidimensional intensity (a), axial intensity (b).

distribution in the focal plane (with coordinates ξ and η) is:

$$E(\xi,\eta) = -\frac{\mathrm{i}l^2}{\lambda f}\mathrm{e}^{-\mathrm{i}kf}\mathrm{e}^{\mathrm{i}k\frac{D+l}{2f}(\xi+\eta)}\mathrm{sinc}\left(k\frac{l\xi}{2f}\right)\mathrm{sinc}\left(k\frac{l\eta}{2f}\right) \times \sum_{h,j=1}^{M}\exp\left[-\mathrm{i}\left(kl\frac{x_h\xi + j\eta}{f} + \phi_{jh}\right)\right], \quad (5)$$

and the intensity is given by $E\overline{E} = |E|^2$, or:

$$I(\xi,\eta) = \left(\frac{l^2}{\lambda f}\right)^2 \mathrm{sinc}^2\left(k\frac{l\xi}{2f}\right)\mathrm{sinc}^2\left(k\frac{l\eta}{2f}\right) \times \left\{\sum_{h,j=1}^{M}\exp\left[-\mathrm{i}\left(kl\frac{h\xi + j\eta}{f} + \phi_{jh}\right)\right]\right\} \times \left\{\sum_{n,m=1}^{M}\exp\left[\mathrm{i}\left(kl\frac{n\xi + m\eta}{f} + \phi_{mn}\right)\right]\right\}. \quad (6)$$

Here $k = 2\pi/\lambda$, λ is the wave length of laser, f is the focal length of the focusing (principal) lens, D is the laser beam diameter, which is assumed to be equal to the RPP total dimension, d is the dimension of the (square) RPP single zone, and ϕ_{mn} is the phase shift which is introduced on a single beamlet by the (m,n) element of the RPP. This term can either be $+1$ or -1 corresponding to a phase shift of 0 or π [6], hence the different beamlets can either be in phase or in phase opposition among themselves.

The analytic solution has two terms: the first corresponds to the analytic solution for a single rectangular aperture, the second is determined by the FT properties.

The first term, the "sinc" function, gives the total envelope of the intensity distribution. It determines the focal spot dimensions and the shape and fraction of the initial laser energy which is contained inside the focal spot (82% in this case). The intensity distribution width is determined by the first zero of the "sinc":

$$\Phi_{\mathrm{S}} = 2\frac{\lambda f}{d}\,. \quad (7)$$

The second term, the summation, represents the "high frequency" modulation of intensity distribution and gives rise to many peaks with typical width

$$\Phi_{\mathrm{p}} = 2\frac{\lambda f}{D}\,. \quad (8)$$

We can see that the spike dimension scales as $1/D$ while the focal spot dimension scales as $1/d$. An example of the obtained focal spot intensity distribution is shown in Figure 2. When we focus the laser beam with the lens only we have hot-spots that have a size smaller but of the same order of the focal spot dimension. By the use of RPP we can control and reduce the peak dimension. The intensity distribution in the focal spot calculated with the simulator described in Appendix A is in a good agreement with Figure 2. Only the analytical solution looks more symmetric than the simulation result. The differences are due to the fact that Fraunhofer approximation requires a slow phase variation [12], but RPP causes a lot of phase-jumps (at the edge of single zones) that limit the accuracy of such approximation. When we use a lens with a large focal length, the approximation is better, and the agreement between the simulation and the analytic calculation improves.

2.2 Hexagonal RPP

The fraction of laser energy contained inside the focal spot is an important parameter in ICF experiments. To improve the energy efficiency of phase plates,

Dixit *et al.* [13] fabricated RPP with hexagonal-shaped elements (see Fig. 3). The central maximum of rectangular aperture far-field pattern contains about 82% of total energy, as we wrote before, while the central maximum of the pattern generated by a plane wave trough a regular hexagonal aperture contains 84% of initial energy, like in an Airy pattern.

We calculated the analytical solution for a hexagonal RPP, as we did for square RPP, in the focal plane of the principal lens, *i.e.* in Fraunhofer approximation.

To simplify our calculations, we made some hypothesis about the dimensions and the position of the zones. We supposed that only external columns and rows contain incomplete zones, that is zones which are cut by the plate edges or only partially illuminated by the laser beam. The global analytical solution contains contributions from complete and incomplete zones, and is given by

$$\begin{aligned} E(\xi,\eta) = {} & E_1(\xi,\eta)\sum_{h=2}^{M-1}\sum_{j=2}^{N-1}\exp\left[-\mathrm{i}\left(kl\frac{x_h\xi+y_j\eta}{f}+\phi_{jh}\right)\right] \\ & + E_2(\xi,\eta)\sum_{h=2}^{M-1}\exp\left[-\mathrm{i}\left(kl\frac{x_h\xi+y_1\eta}{f}+\phi_{1h}\right)\right] \\ & + E_3(\xi,\eta)\sum_{h=2}^{M-1}\exp\left[-\mathrm{i}\left(kl\frac{x_h\xi+y_N\eta}{f}+\phi_{Nh}\right)\right] \\ & + E_4(\xi,\eta)\sum_{j=2}^{N-1}\exp\left[-\mathrm{i}\left(kl\frac{x_1\xi+y_j\eta}{f}+\phi_{j1}\right)\right] \\ & + E_5(\xi,\eta)\sum_{j=2}^{N-1}\exp\left[-\mathrm{i}\left(kl\frac{x_M\xi+y_j\eta}{f}+\phi_{jM}\right)\right] \\ & + E_6(\xi,\eta)\exp\left[-\mathrm{i}\left(kl\frac{x_1\xi+y_1\eta}{f}+\phi_{11}\right)\right] \\ & + E_7(\xi,\eta)\exp\left[-\mathrm{i}\left(kl\frac{x_1\xi+y_N\eta}{f}+\phi_{N1}\right)\right] \\ & + E_8(\xi,\eta)\exp\left[-\mathrm{i}\left(kl\frac{x_M\xi+y_1\eta}{f}+\phi_{1M}\right)\right] \\ & + E_9(\xi,\eta)\exp\left[-\mathrm{i}\left(kl\frac{x_M\xi+y_N\eta}{f}+\phi_{NM}\right)\right], \end{aligned} \tag{9}$$

where l is the diameter of the circle circumscribing an hexagonal, $N \times M$ is the number of zones in the RPP, (x_h, y_j) are the coordinates of the center of zones, (ξ, η) are the coordinates in the focal plane and again ϕ_{mn} is the phase shift which is introduced on a single beamlet by the (m, n) element of the RPP.

Here, the principal term E_1 represents the contribution of complete zones, (the complete solution and the expression for all the terms E_i may be found in Ref. [14]), and

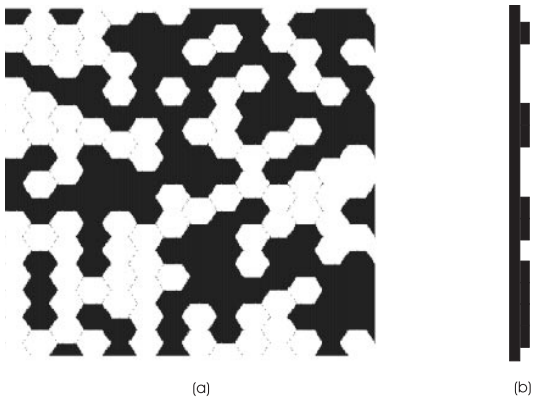

Fig. 3. Front and side view of a RPP with hexagonal zones. Black and white zones are in reality equally transparent, but white zones do not introduce additional phase, black zones introduce an additional phase of $\lambda/2$.

is given by

$$\begin{aligned} E_1(\xi,\eta) = {} & -\frac{\mathrm{i}}{\lambda f}\mathrm{e}^{-\mathrm{i}kf}\left\{\frac{\sqrt{3}}{4}l^2\mathrm{sinc}\left(\frac{kl\xi}{4f}\right)\mathrm{sinc}\left(\frac{k\sqrt{3}l\eta}{4f}\right)\right. \\ & -\frac{lf}{2k\eta}\left[\sin\frac{kl}{8f}\left(\xi+\sqrt{3}\eta\right)\mathrm{sinc}\frac{kl}{8f}\left(\xi+\sqrt{3}\eta\right)\right. \\ & \left.\left. -\sin\frac{kl}{8f}\left(\xi-\sqrt{3}\eta\right)\mathrm{sinc}\frac{kl}{8f}\left(\xi-\sqrt{3}\eta\right)\right]\right\}. \end{aligned} \tag{10}$$

The terms $E_2 \ldots E_9$ represent the contribution of incomplete zones, those lying at the four sides and the four angles of the phase plate. Then E_2 is the contribution of the generic incomplete hexagonal zones of the first row of the RPP from the second to the $M-1$ zone, E_6 is relative to the first element of the RPP (first row, first column), E_8 represents the last zone of the first row; E_3 is relative to the last row, E_7 represents the contribution of the element on the first column and last row of the RPP, E_9 is relative to the element on the last column and last row; E_4 represents the contribution of the generic incomplete hexagonal zone of the first column and E_5 the contribution of the generic incomplete hexagonal zone of last column. Notice that each E_i term is proportional to the total area of hexagonal zones which have produced it.

Equation (10) contains two terms, the first represents the envelope of the entire solution and it given by Fraunhofer diffraction of a hexagonal fenditure. The energy focused inside such an envelope is about 84%, as we expected. The dimension of focal spot is determined by the first zero of the "sinc" function:

$$\Phi_{\mathrm{S}} = 2\frac{4}{3}\frac{\lambda f}{l}\,. \tag{11}$$

The exponential factors following $E_1 \ldots E_9$ represent the "high spatial frequency" modulation of RPP. The spikes dimension is determined by the exponential and is:

$$\Phi_{\mathrm{p}} = 2\frac{\lambda f}{D}\,. \tag{12}$$

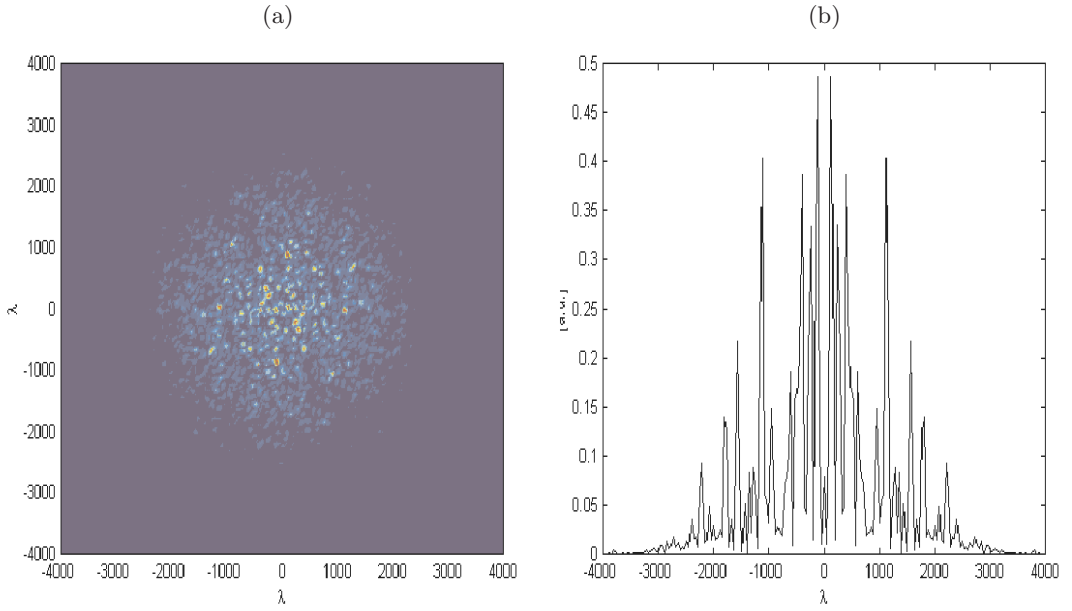

Fig. 4. Focal spot intensity distribution, analytically calculated, with a hexagonal RPP of 1 688 zones. RPP dimensions are $49\,500\lambda \times 47\,650\lambda$ and $l = 1\,500\lambda$, $f = 3 \times 10^6\lambda$. Bidimensional intensity (a), axial intensity (b).

Figure 4 shows the intensity distribution calculated from equation (9). Again it is possible to show that there is good agreement with the intensity distribution obtained with the simulator in the same conditions (the same considerations about the differences between simulation and the analytical solution as in the square RPP case can be made).

2.3 Figure of merit

In order to evaluate the design of RPP we made the Fourier transform of the intensity distribution in the focal spot plane. Figure 5 shows such FT for the case of a square RPP analytically calculated from equation (6). The situation is similar in the case of hexagonal RPPs (FT of "sinc" function convoluted with sums of Dirac delta functions).

Figure 5 shows the presence of a maximum spatial frequency equal to the inverse of the spike width, as expected. Of course the design of RPP must be done so that such spike width is shorter than the plasma electron mean-free-path, but this condition is not sufficient. Indeed Figure 5 shows the presence of secondary, local maxima at spatial frequencies which are multiple of the inverse of the spot dimension. Other secondary maxima may appear because the design of the RPP is not really random but contains some long-distance correlation. All such secondary maxima represent energy concentration on long scale lengths and must hence be minimized (which corresponds to maximizing the evaluation parameter J described in the introduction).

The maximum at zero-frequency, due to FT properties, represents the total energy in the focal spot. As we could expect the maximum frequencies are related to spike dimension: as we increase the number of zones in a RPP (either hexagonal or rectangular) we obtain a higher maximum frequency and the local maxima, at lower frequencies are smaller. This corresponds to a larger concentration of energy in short scale spikes.

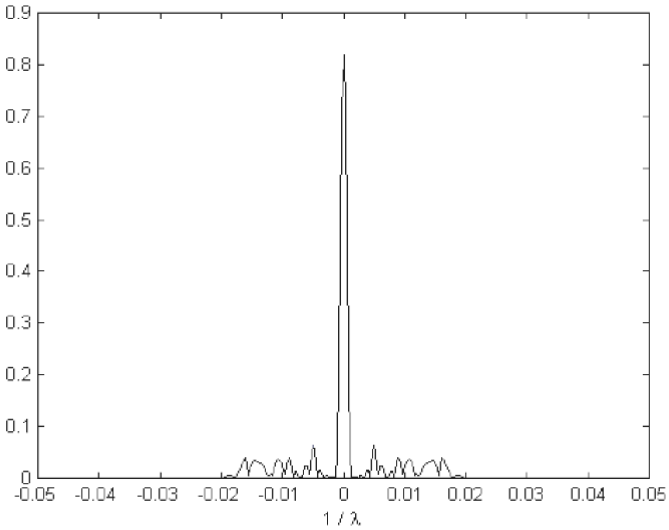

Fig. 5. Analytical FT of the intensity distribution in the focal spot obtained with a square RPP (shown in Fig. 2). In this figure we report the x-axis distribution of the 2D FT analytically calculated from equation (6).

We applied equation (2) with RPPs and obtained that J increased with the number of zones. This result can appear obvious, but this is true only if the 0-phase and the π-phase zones are randomly distributed, as we verified on a simple RPP (8×8 zones) with a different position of two types of zones. In this case we noted that J increased when zones are more randomly distributed (and this will be truer with a large number of zones). See later (Sect. 3.3) same discussion for PZPs and Figure 10.

3 Phase zone plates

Phase zones plates consist of an array of Fresnel lenses [7,9]. A transparent Fresnel lens is made of transmitting

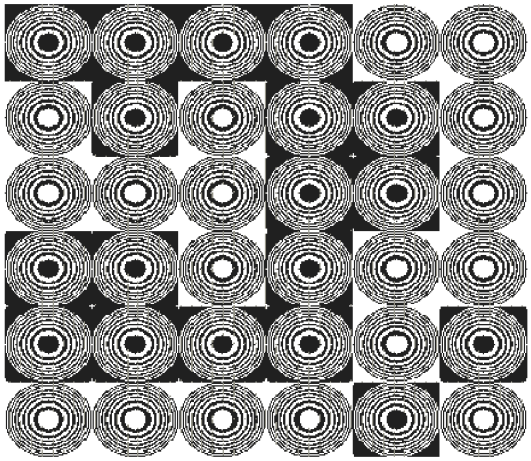

Fig. 6. Square PZP. Black and white zones are in reality equally transparent, but white zones do not introduce additional phase, black zones introduce an additional phase of $\lambda/2$.

zones, alternately with 0-phase and π-phase. Rings are concentric and their dimensions are chosen so that the contribution from each single zone is in phase with all the others in the focal plane. All the Fresnel lenses in a PZP are of the same dimension and contain the same number of zones, but there are two kinds of Fresnel lenses: with a first zone with 0-phase and with a first zone with π-phase. The focal length (f_z) of this lens, its dimension (r_N) and the number of zones (N) are related [15,16] through:

$$r_N = \sqrt{N\lambda f_z}. \tag{13}$$

PZPs work with a principal focusing lens and, like in RPPs, when a beam travels through a PZP is split into several beamlets. The shape of focal spot is determined by the shape of each individual beamlet, that can be square or hexagonal. The focusing lens and the Fresnel lens are an optical device with a total focal length:

$$\frac{1}{f_{\mathrm{TOT}}} = \frac{1}{f_Z} + \frac{1}{f}\,. \tag{14}$$

In the focal plane (at distance f_{TOT}) there is an array of foci, each beamlet being focused in a different point. In the principal focal plane (at distance f) each beamlet is defocused and enlarged and then will overlap with the others. The dimension of the focal spot in this plane is [7,9]:

$$W_{\mathrm{S}} \simeq W_z \frac{f}{f_z} = 2\sqrt{\frac{N\lambda}{f_z}} f = 4\frac{N\lambda}{W_z} f, \tag{15}$$

where $W_z = 2r_N$ is the diameter of the single Fresnel lens.

Energy efficiency is about 81%. PZPs can produce an average profile which is almost flat-top (super-Gaussian-like). Such flat irradiation is very suitable for a series of experiments including laser plasma interaction and laser shock experiment.

3.1 Square PZP

We calculated the analytical solution of a plane wave traveling through a square PZP in Fraunhofer approximation, and we compared it with simulation results. To simplify analytical calculations we considered only Fresnel lenses with complete zones, and only complete Fresnel lenses in the PZP (see Fig. 6). The phase plate is an array of $M \times M$ Fresnel lenses, each of dimension W_z, where $MW_z = D$, inserted in a square cell. The contribution of a single Fresnel lens to the electric field in the focal plane is:

$$E^q_{\mathrm{PZP}}(\xi,\eta) = \\ -\frac{\mathrm{i}}{\lambda f}\mathrm{e}^{-\mathrm{i}kf} W_z^2 \mathrm{sinc}\left(k\frac{W_z\xi}{2f}\right)\mathrm{sinc}\left(k\frac{W_z\eta}{2f}\right) + 2\frac{\mathrm{i}k}{f}\mathrm{e}^{-\mathrm{i}2kf} \\ \times \sum_{n=0}^{\frac{N-1}{2}} \frac{r_{2n+1}J_1\left(r_{2n+1}k\frac{\xi^2+\eta^2}{f}\right) - r_{2n}J_1\left(r_{2n}k\frac{\xi^2+\eta^2}{f}\right)}{k\frac{\xi^2+\eta^2}{f}}, \tag{16}$$

where $k = 2\pi/\lambda$, J_1 is the Bessel function and the index q indicates the square shape of the lens. Hence, the intensity profile produced from a complete PZP is:

$$I(\xi,\eta) = |E^q_{\mathrm{PZP}}|^2 \left\{\sum_{r,s=1}^{M} \exp\left[-\mathrm{i}\left(kW_z\frac{r\xi+s\eta}{f} + \phi_{sr}\right)\right]\right\} \\ \times \left\{\sum_{j,h=1}^{M} \exp\left[\mathrm{i}\left(kW_z\frac{h\xi+j\eta}{f} + \phi_{jh}\right)\right]\right\}. \tag{17}$$

The term $|E^q_{\mathrm{PZP}}|^2$ represents the overall envelope of the intensity profile in focal plane and determines the total dimension of the focal spot (see Eq. (15)). The analytical solution given by equation (16) is less significant than the one obtained for RPP. Indeed, as already said in this case, the analytical solution requires a slow variation of the phase over the integration domain. But in PZPs there are many more phase jumps so that the analytical solution corresponds to the case of very long focal lengths

As in the case of PZPs, the dimension of hot-spots is given by equation (8). However here relation between focal spot dimension and peaks dimension is different. In the case of RPPs, this is given by the ratio between equation (8) and equation (7):

$$\frac{\Phi_{\mathrm{p}}}{\Phi_{\mathrm{S}}} = \frac{d}{D} = \frac{1}{M}\,. \tag{18}$$

In the case of the PZP it is instead given by the ratio between equation (8) and equation (15):

$$\frac{\Phi_{\mathrm{p}}}{W_{\mathrm{S}}} = \frac{2W_z}{ND} = \frac{2}{NM}\,. \tag{19}$$

In Figure 7 we report an intensity profile obtained from simulation in the principal focal plane while Figure 8 shows the intensity profile in a plane 5 mm beyond the principal focal plane.

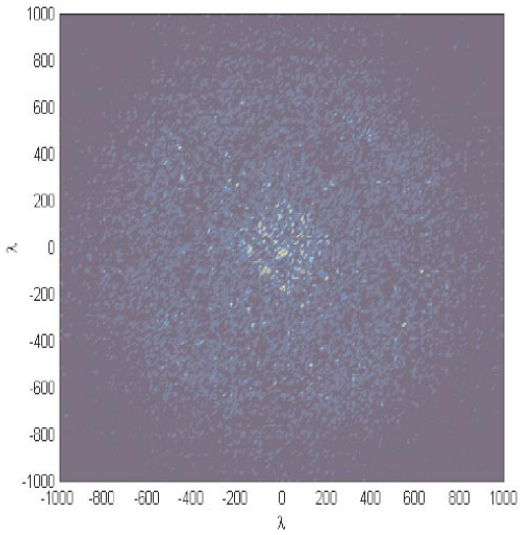

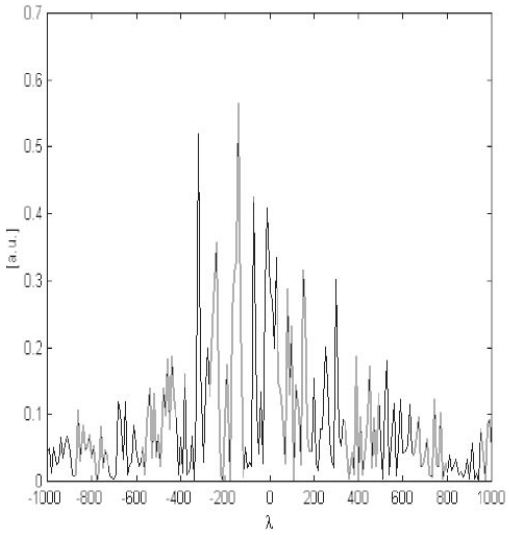

Fig. 7. Calculated distribution of intensity in the principal focal plane with a square PZP, with dimensions $W_z = 10^4\lambda$, $D = 96 \times 10^3\lambda$ ($M = 9$ complete Fresnel lenses), $N = 6$ complete zones for each Fresnel lens, $f_z = 4.17{\times}10^6\lambda$ and $f = 750{\times}10^3\lambda$. Focal spot dimension is $1\,800\lambda$, and hot-spots dimension is 15.6λ.

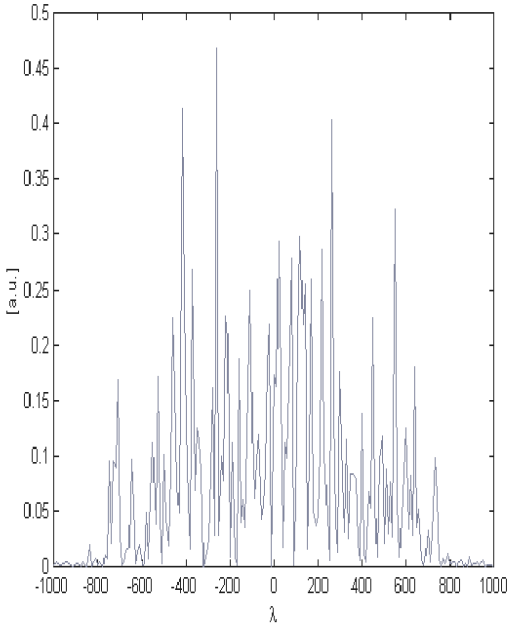

(a)

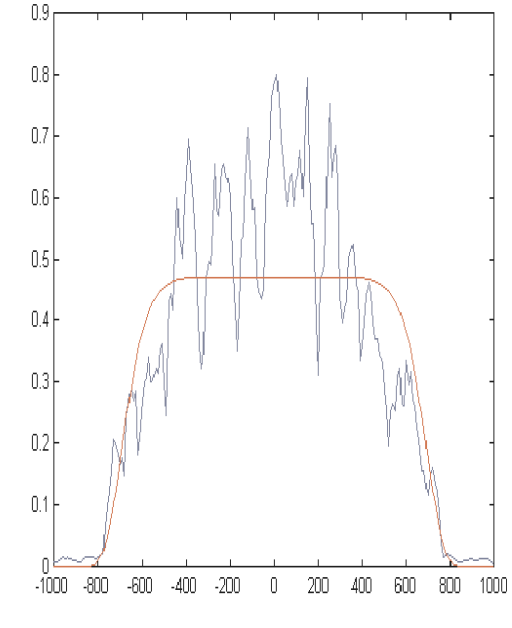

(b)

Fig. 8. Calculated distribution of intensity in the principal focal plane with a square PZP, with dimension $W_z = 10^4\lambda$, $D = 96 \times 10^3\lambda$ ($M = 9$ complete Fresnel lenses), $N = 6$ complete zones for each Fresnel lens, $f_z = 4.17 \times 10^6\lambda$ and $f = 750 \times 10^3\lambda$. This optimal plane is $5 \times 10^3\lambda$ beyond principal focal plane. Intensity profile along one focal spot diameter (a), spatially filtered intensity profile compared with a super-Gaussian (b). The super-Gaussian conserves the total energy contained in the initial intensity distribution.

As already pointed out in previous works [6,9,13] the intensity distribution in the focal plane of the main lens (at distance f) is characterized by a central peak in the origin of axis ($\xi = \eta = 0$). This peak arises because of the zeroth order diffraction contributions. In the first approximation the E_i terms are proportional to the total area of zones that produced it. Now, since the summation term depends only on the terms ϕ_{jh} and such values can be either 1 or -1 (if we take care of make differential phase equal to π), then, in principle, we can eliminate the central peak by making PZPs with an equal area of 0-phase and π-phase zones. However, this is very difficult to be practically realized because the fabrication accuracy at the zones edge should be the same order of wave length of the laser beam, and because some of our assumptions are not strictly true (in particular not all the zones are completely illuminated by the laser beam). This discussion is also true for RPPs.

Then, to reduce the central peak, we also need to work out of focal plane: here a little defocusing will cause a non-complete beamlet overlapping and elimination of zeroth order diffraction. The dimension of focal spot in this plane will be

$$W_{\mathrm{S}} = W_z \frac{(f+\delta) - f_{\mathrm{TOT}}}{f_{\mathrm{TOT}}}, \tag{20}$$

where δ is the distance from the principal focal plane, W_{S} is practically equal to W_z. At bigger distances the average intensity assumes a Gaussian profile, as already pointed out in references [7,9].

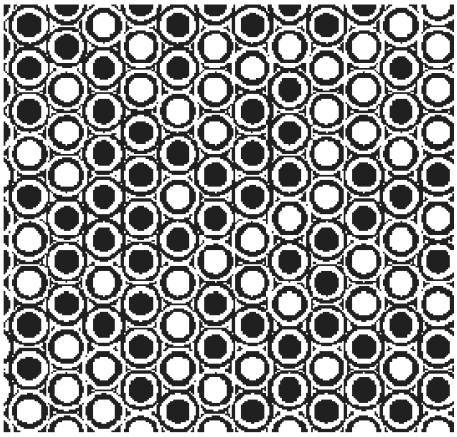

Fig. 9. Hexagonal phase zone plate. Black and white zones are in reality equally transparent, but white zones do not introduce additional phase, black zones introduce an additional phase of $\lambda/2$.

3.2 Hexagonal PZP

Fresnel lenses can be placed in an hexagonal cell, each cell is surrounded by 6 cells, to obtain a focal spot shape which is approximately circular [7] (see Fig. 9). Also, in this way, in each Fresnel lens, the area filled by incomplete zones is lower than with square cell, so that the PZP becomes more efficient

The analytical solution for the electric field, in the focal plane, for a planar wave traveling through a single hexagonal cell is

$$E^h_{\mathrm{PZP}}(\xi,\eta) = E_1(\xi,\eta) - 2\frac{\mathrm{i}k}{f}\mathrm{e}^{-\mathrm{i}2kf} \times \sum_{n=0}^{\frac{N-1}{2}} \frac{r_{2n+1}J_1\left(r_{2n+1}k\frac{\xi^2+\eta^2}{f}\right) - r_{2n}J_1\left(r_{2n}k\frac{\xi^2+\eta^2}{f}\right)}{k\frac{\xi^2+\eta^2}{f}} \tag{21}$$

where $E_1(\xi,\eta)$ is given in equation (10). To simplify the analytical calculations we considered only Fresnel lenses with complete zones and we considered complete Fresnel lenses only. The intensity distribution is like in equation (17), where term E^q_{PZP} is replaced by E^h_{PZP} (Eq. (21)).

In this case too, the term $\left|E^h_{\mathrm{PZP}}\right|^2$ represents the total envelope of the intensity distribution. Focal spot and hot-spots dimensions are given by equation (15) and equation (8) respectively.

3.3 Figure of merit

As explained before, we introduced another figure of merit to analyze the intensity profile quality produced by a PZP. For PZP we have to consider both J (Eq. (2)) and J_2 (Eq. (3)).

Even without explicitly making the FT of equations (16, 21), we can deduce that the FT is limited and has negligible values at spatial frequency above $D/\lambda f$. Equation (17) contains three terms and its FT is a convolution of the FT of the three terms: the FT of the two exponential summation is a summations of Dirac deltas and the maximum spatial frequency is $(M-1)W_z/\lambda f$; the maximum frequency of the FT of the first term is $W_z/\lambda f$ (is a sum of "sinc" functions and Bessel functions, whose bidimensional FT are respectively square and circular functions). Then the "global" maximum frequency is the maximum frequencies of the three terms and hence is $D/\lambda f$.

With PZP we can vary different parameters: number of Fresnel lenses (M), the number of zones in a single lens (N) and the focal length of Fresnel lenses (f_z). Two of these can be chosen independently, the third one is then fixed by equation (13) and the fact that $MW_z = M(2r_n) = D$.

As for the other parameters, λ and D are constant since in practice they depend on the laser beam characteristics, and f must be changed so to maintain a constant dimension for the focal spot (see Eq. (15)).

We analyzed three cases: variation of M (5, 6, 8, 10, 12), N constant = 4; N changes (3, 4, 5, 8) and M constant = 10; M and N change and f_z constant. In the first two cases J and J_2 increase with increasing of M or N. In the last case J_2 shows a maximum. The average profile depends on the number M of Fresnel lenses in a PZP: if this is low the average intensity does not reach a super-Gaussian shape. J depends instead, as before, on the number N of zones in each Fresnel lenses. These results are true if there is a random disposition of the two types of Fresnel lenses, both figures increasing as disposition gets more and more random (see Fig. 10). These different aspects have to be optimized: first of all we choose the number of Fresnel lenses that give the desired flat-top profile, after we choose the number of zones in order to have peaks dimensions which are short enough (not to affect energy deposition on target).

A comparison between rectangular and hexagonal PZP shows that the last ones are more efficient, having a greater number of complete zones with the same dimension of lenses.

4 Hot-spots suppression

In the previous sections, we analyzed the effects of phase plates on planar waves. In this section we show that phase plates can suppress hot-spots whenever they are present in the laser beam.

Figure 11 shows the intensity profile at the initial plane and the hot-spots generated in the focal spot with only a focusing lens ($f = 500$ mm). The initial intensity distribution was randomly generated as a sum of Gaussians with random height and position. Also the phase of the initial beam was generated as sum of random Gaussian. Wavelength is 0.543 μm, dimensions are 40 mm $\times$ 40 mm.

The intensity profile obtained with an hexagonal PZP and the initial beam of Figure 11 is depicted in Figure 12. Fresnel lenses dimension is 13 mm, their number is 23

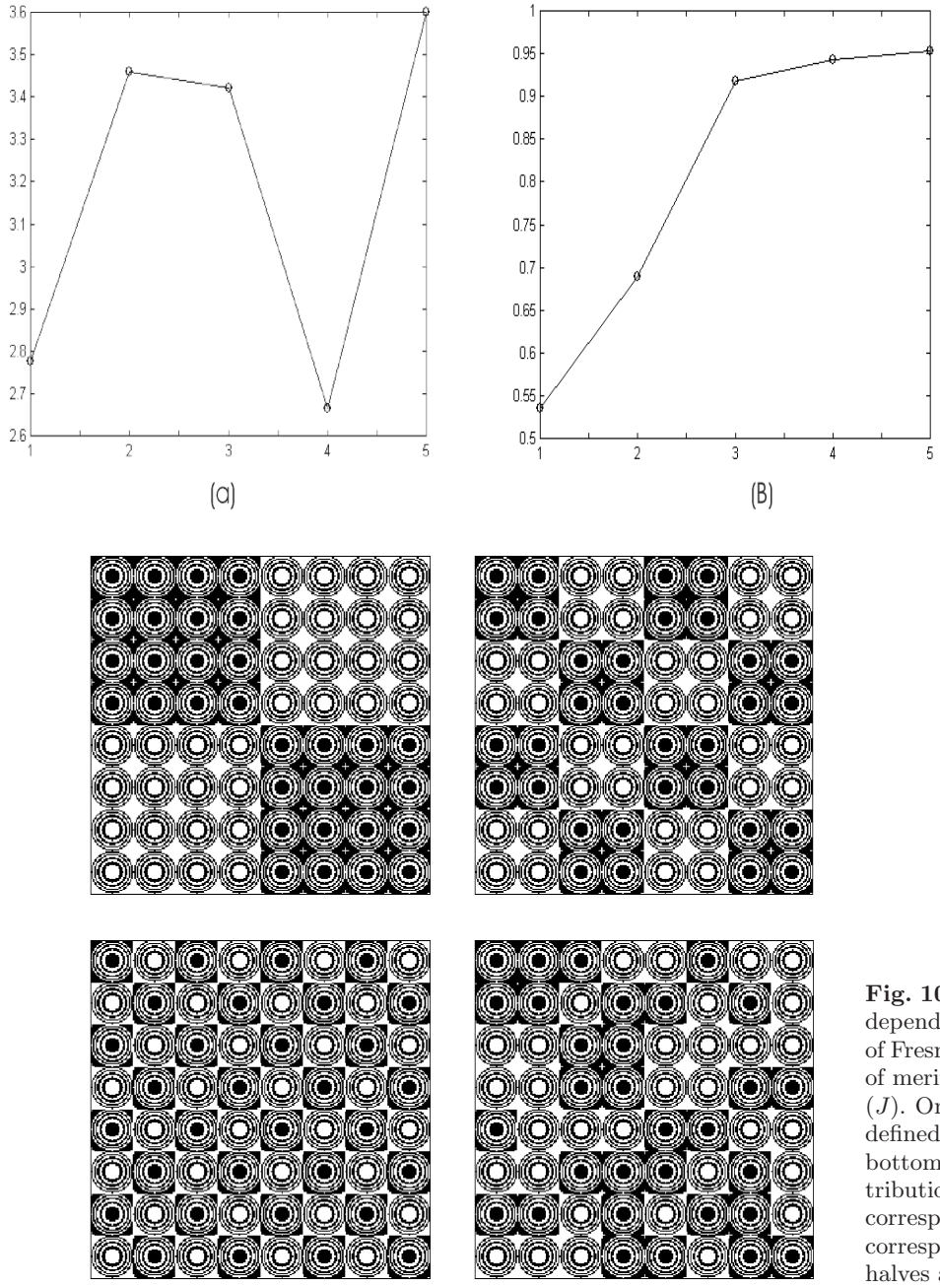

Fig. 10. Shape of the two figures of merit depending on the position of the two types of Fresnel lenses. On the left side the figure of merit defined in equation (2) is showed (J). On the right side the figure of merit defined in equation (3) is showed (J_2). The bottom part of the figure shows the distribution of the Fresnel lenses in the PZP corresponding the different point. Case 1 corresponds to the plate divided in two halves and it is not showed.

and their focal length is 10 m. Each Fresnel lens contains 8 completes zones. Again, the focal length of the focusing lens is 500 mm. From equation (15) we obtain a spot dimension of 650 μm, with peaks of 13.6 μm.

Figure 12 clearly shows how phase plates can suppress hot-spots, generating a focal spot characterized by small peaks will do not affect energy deposition on target.

5 Experimental results

We compared our simulations with experimental results obtained with the Asterix laser at Max-Planck-Institut für Quantenoptik in Garching.

Asterix is a high power single-mode iodine laser with emission wavelength at 1.315 μm, and a maximum energy of 1.2 kJ per pulse. The laser light was converted with nonlinear KDP crystals into third harmonics ($\lambda = 438$ nm), with an energy conversion efficiency of 56%. Pulse duration was 400 ps (producing a 3 TW power full-energy laser shots) with a duty cycle of 20 minutes between two laser shots. The diameter of beam is 300 mm.

In the experiment, first we obtained the images of laser intensity distribution at various focal planes through hexagonal PZP. Then we irradiated solid Al targets (foils with a typical thickness of 18 μm) in order to produce a high pressure shock in the material. Shock breakout was

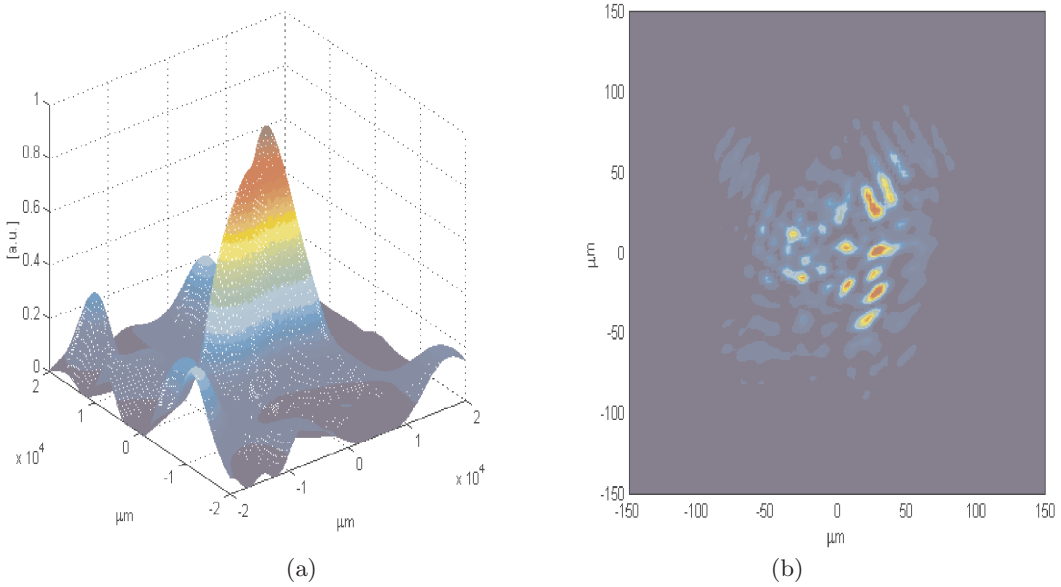

Fig. 11. Simulation of hot spots. Initial intensity profile, the wavelength is $\lambda = 0.543$ μm and the dimensions are 40 mm $\times$ 40 mm (a). Intensity profile at focal plane ($f = 500$ mm) (b).

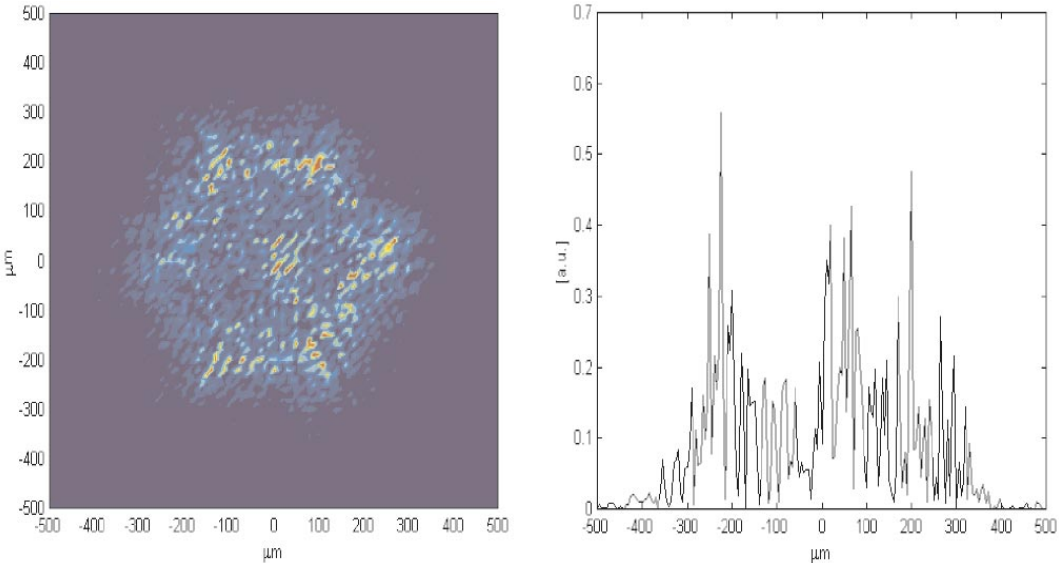

Fig. 12. Intensity profile in the principal focal plane with a hexagonal PZP ($D = 40$ mm, $f = 500$ mm, $W_z = 13$ mm, $f_z = 10$ m and $N = 8$, with 23 Fresnel lenses), the initial beam is the same of Figure 11. We obtain $W_S = 650$ μm and $\Phi_p = 13.6$ μm.

detected from target rear side. The uniformity of the shock is connected to the uniformity of the irradiation profile, giving an experimental evidence of laser profile effects as shown for instance in [17,18]. The experimental setup in this case is shown in Figure 13. A streak camera is used to record shock breakout images. When the intensity distribution had to be obtained, the target was removed. In this case we used a cw He:Cd laser operating at the same (3ω) wavelength, expanded to get a 30 cm diameter. The diagnostic system consisted in a CCD camera with pixel size of 20 μm coupled to a magnifying imaging system with a magnification $M = 10$. The system spatial resolution was 2 μm.

The hexagonal PZP had dimension of Fresnel lenses (W_z) of 20 mm, focal length (f_z) of 28.2 m with 8 complete zones. The focusing lens had a focal length of 564 mm and the focal spot was of 0.4 mm. Due to technical problems with the lithography process, it was not

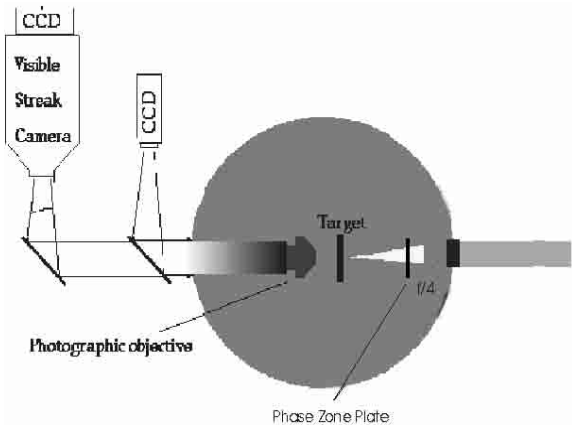

Fig. 13. Experimental set-up, used at MPQ to detect shock breakout from laser irradiated Al targets.

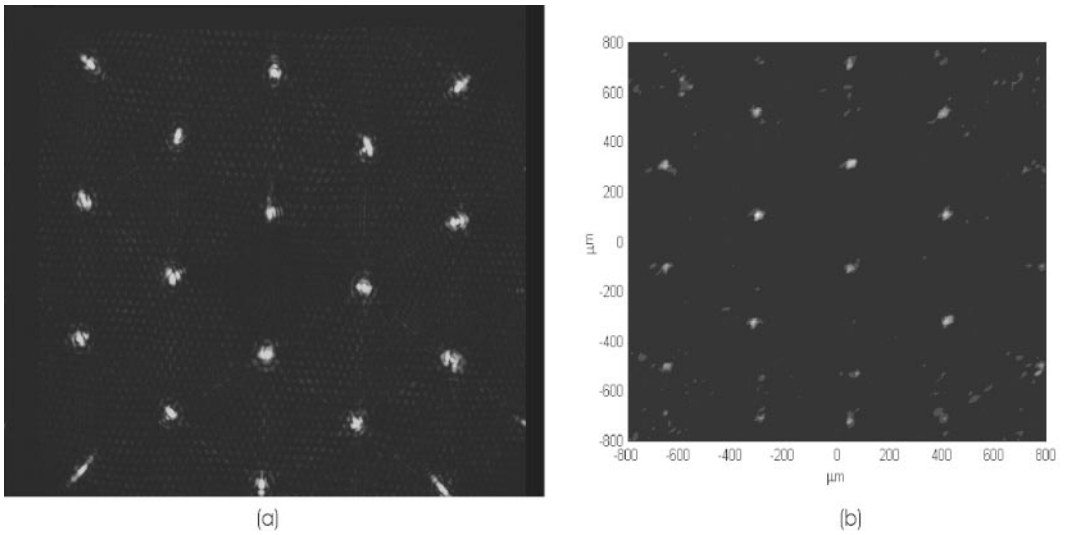

Fig. 14. Intensity distribution in the total focal plane. The laser characteristics were $D = 300$ mm and $\lambda = 44$ nm, the focal length of principal lens was $f = 564$ mm. PZP characteristics were $W_z = 20$ mm, $f_z = 18\,100$ mm and $N = 8$. Experimental distribution (a), simulated distribution (b).

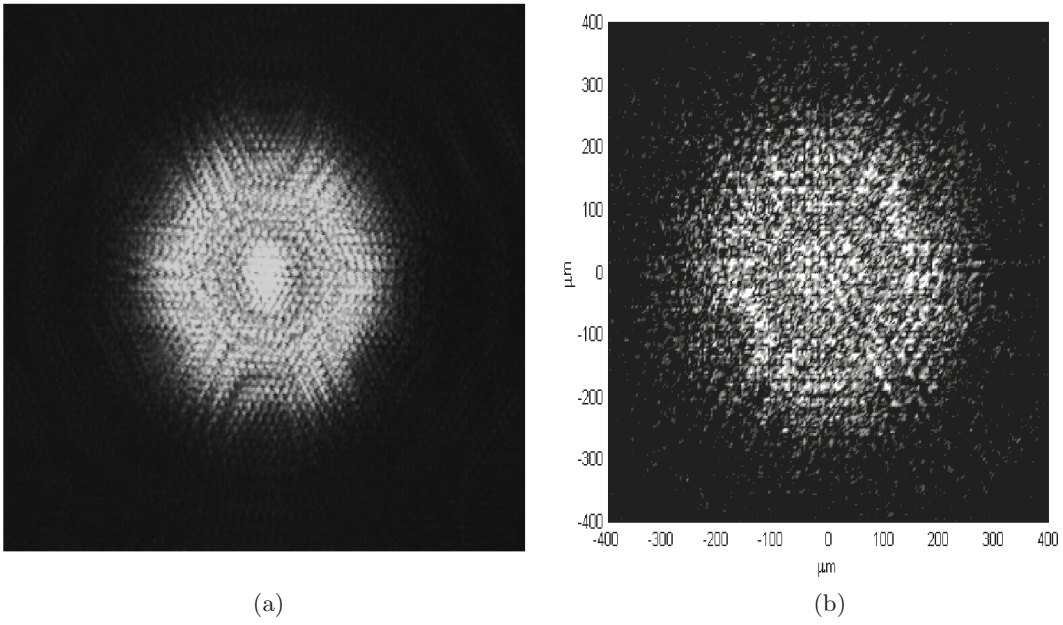

Fig. 15. Intensity distribution in the principal focal plane. Same laser, PZP and lens characteristics as in Figure 14. Experimental distribution (a), simulated distribution (b).

possible to produce a PZP large enough to accommodate the Asterix laser beam. Hence we designed a PZP which had to be placed at distance $f/4$ from the target and $3f/4$ from the focusing lens. In this case the beam diameter was reduced to $\simeq 7.5$ cm allowing a single PZP to be used. The laser flux at position $f/4$ was 637 mJ/cm^2. The theoretical value of damage threshold for the coating on which the Fresnel lenses are etched is of the order of a couple of J/cm^2. Indeed the PZP did not suffer any resist damage even at distance $f/4$. After $\simeq 50$ high energy shots, some damages began to be evident. We think however that this was mainly due the plasma and debris emission from the target. Results in this paper show how this configuration works equally well. Attempts to use larger PZPs obtained by successive lithography of 4 different PZPs onto a single fused silica plate did not work: the phase aberration introduced at the edges of each PZP completely destroyed PZP effectiveness.

To perform the simulations we used a beam with a Gaussian initial distribution in intensity and whose phase was a sum of random Gaussians:

$$\phi(r) = \sum_{i=1}^{30} A_i \exp\left(-\frac{(r - r_i)^2}{2\sigma_i^2}\right), \qquad (22)$$

to obtain a random but correlated phase distribution. Simulations with an initial phase constant over the all laser beam give similar results, the changes mainly affect peak positions, not their height. This is what we expected, because, in order to suppress hot-spots using phase plates, we want to get an intensity profile at focal spot with a phase which is practically uncorrelated with the initial phase of the beam.

Figures 14 and 15 show the comparison between experimental images (a) and simulations (b) in different planes,

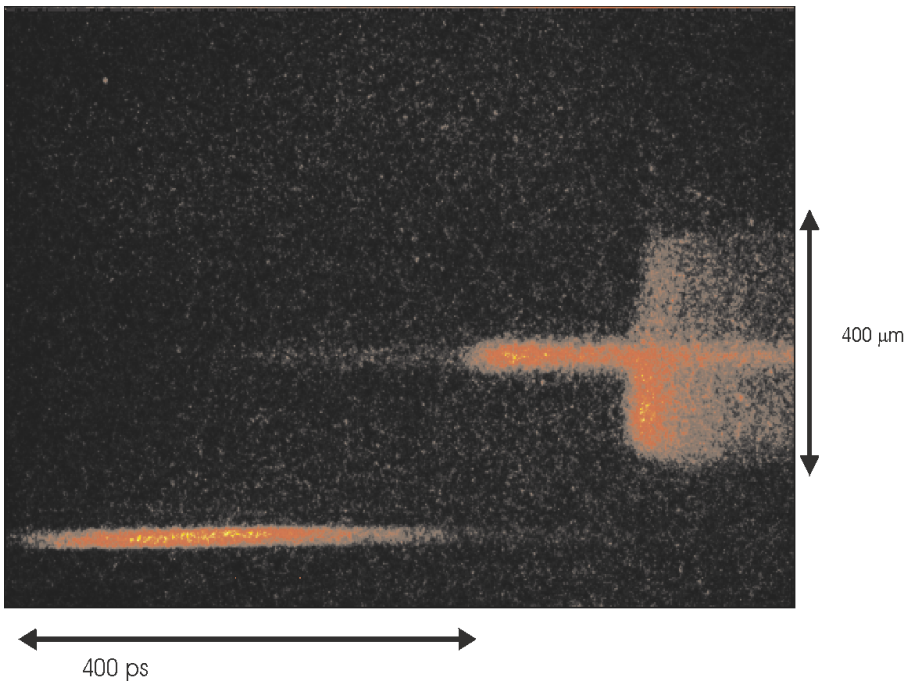

Fig. 16. Shock breakout image corresponding to the intensity distribution in Figure 15. The target was 18 μm Al. The energy pulse was 300 J. Notice the central peak in shock wave.

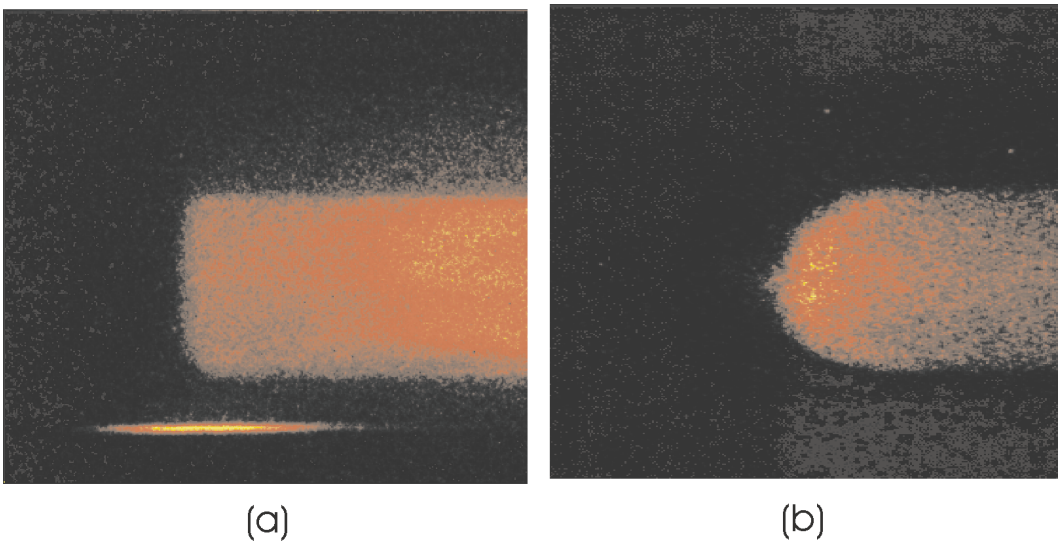

Fig. 17. (a) Shock breakout image corresponding to the intensity distribution in the optimal plane. The shock breakout is flat. The target was 18 μm Al. (b) Shock breakout image corresponding to the intensity distribution beyond the optimal plane the target was 18 μm Al. The shock breakout have a Gaussian shape.

i.e. the focal plane of the total system (focusing lens + PZP) and in the principal focal plane (the focal plane of the focusing lens). In order to get a closer comparison, the images obtained from the simulation were treated to take into account the finite size of the CCD camera pixels used in the experiment.

Finally Figures 16 and 17 show the shock front from Al targets put in the position corresponding to the intensity distribution of Figure 15 in the optimal plane, where a flat top distribution is achieved, and beyond that plane, where the average intensity has a Gaussian-like profile. It is very easy to see the effect of the central peak in the principal focal plane, as well as the curved shock front when the intensity distribution becomes Gaussian-like.

6 Conclusions

In this paper we studied the intensity profile generated by the use of phase plates and we analyzed the dependence of peak size and average intensity profile on the characteristic of phase plates.

We considered random phase plate and phases zone plate. While both can suppress hot-spots in the focal spot, PZPs can also produce an average intensity profile which is super-Gaussian-like, hence producing a more homogeneous irradiation. This aspect is advantageous even if the energy efficiency is lower for PZPs than for RPPs (the focal spot contains only 81% of the total laser energy against 84% of the hexagonal RPP case).

We acknowledge the useful discussions with Sergio Bittanti and Fabio Previdi, Dipartimento di Elettronica e Informazione, Politecnico di Milano, Italy. We also thank Colin Danson and Dave Pepler, Rutheford Appleton Laboratory, UK for the discussion on the PZP technique and for having produced the PZPs used in the experiment at MPQ. Finally we thank Michel Koenig and Alessandra Benuzzi with whom the experiment at MPQ has been realised.

Appendix A: Numerical Simulator

The analytical solutions derived in Sections 2.1, 2.2, 3.1 and 3.2 are only available in the lens focal plane, thanks to the FT properties. In order to get the field and intensity distribution in all others planes, we needed to develop a specific numerical simulator. This also allows to use an initial condition (field incident on phase plate) with any phase and amplitude distribution.

The simulator is based on Fresnel equation [10] and hence works in the Fresnel approximation, and not only in Fraunhofer approximation. This requires to solve the double integral:

$$E(\mathbf{r}_0) = -\frac{\mathrm{i}}{2\lambda}\int\int_A (1+\cos\theta)\,\frac{E_i(\mathbf{r})\,\mathrm{e}^{-\mathrm{i}\mathbf{k}\cdot\mathbf{R}}}{R}\mathrm{d}A, \qquad (23)$$

where

A is the integral domain representing the region where there is a non-null incident wave;
$\mathbf{r}$ is a point on the integral domain;
$\mathbf{r}_0$ is the point where we calculated the integral;
$\mathbf{R} = \mathbf{r}_0 - \mathbf{r}$;
$1+\cos\theta$ is the obliquity factor, where θ is the angle between the normal at front wave surface and the vector $\mathbf{R}$.

In order to solve equation (23) we used a 9-points bidimensional Simpson numerical method [19], that is an extension of the polynomial monodimensional Simpson method [20].

We compared numerical simulations with known analytical solution (diffraction from simple geometry fenditure in Fraunhofer approximation) to validate our simulator. In all cases we got a very good agreement [14].

Optical devices as focusing lens and phase plates introduce a phase difference that has to be included in the exponential term in equation (23).

To predict integration error we must analyze the 4th order of derivation of the integrated function, which implies a non-simple calculus. However errors mainly depend on the initial phase (sum of initial beam phase and phase difference introduced by optical devices). Furthermore we have to consider errors due to the numerical approximations. To evaluate the error we analyzed the difference between simulation results obtained with different integration steps. We then reduced the step until the difference between results obtained with two successive integration steps was close to zero (*i.e.* small then a parameter fixed *a priori*).

References

1. J. Nuckolls, L. Wood, A. Thiessen, G. Zimmerman, Nature **239**, 139 (1972).
2. C. Yamanaka, *Introduction to laser fusion* (Harwood Academic Publisher, Chur, 1991).
3. J. Lindl, Phys. Plasmas **2**, 3933 (1995).
4. S. Atzeni, Laser Part. Beams **9**, 233 (1991)
5. S. Skupsky, K. Lee, J. Appl. Phys. **54**, 3362 (1983).
6. Y. Kato, K. Mima, N. Miyanaga, Phys. Rev. Lett. **53**, 1057 (1984).
7. R.M. Stevenson *et al.*, Opt. Lett. **19**, 363 (1994).
8. T.H. Bett *et al.*, Appl. Opt. **34**, 4025 (1995).
9. I.N. Ross, D.A. Pepler, C.N. Danson, Opt. Commun. **116**, 55 (1995).
10. M. Born, E. Wolf, *Principles of Optics* (Pergamon Press, Oxford, 1975).
11. L. Amerio, *Analisi Matematica II* (UTET, Torino, 1992).
12. R. Guenther, *Modern Optics* (John Wiley & Sons, New York, 1990).
13. S.N. Dixit *et al.*, Appl. Opt. **32**, 2543 (1993).
14. C. Bleu, Laurea thesis, Politecnico di Milano, Milano, December 1999.
15. M. Sussman, Am. J. Phys. **28**, 394 (1960).
16. D.J. Stigliani, R. Mittra, R.G. Semonin, J. Opt. Soc. Am. **57**, 610 (1967).
17. M. Koenig, B. Faral, J.M. Boudenne, D. Batani, S. Bossi, A. Benuzzi, Phys. Rev. E **50**, 3314 (1994).
18. D. Batani, A. Balducci, D. Beretta, A. Bernardinello, Th. Lower, M. Koenig, A. Benuzzi, B. Faral, T. Hall, Phys. Rev. B **61**, 9287 (2000).
19. P.J. Davis, P. Rabinowitz, *Methods of numerical integration* (Academic Press, Orlando, 1984).
20. L. Gotusso, *Calcolo numerico* (CLUP, Milano, 1978).